The influence of ion flux on defect production in MeV proton-irradiated silicon

A. Hallén, D. Fenyö, and B. U. R. Sundqvist
Department of Radiation Sciences, Division of Ion Physics, P.O. Box 535, Uppsala University, S-751 21 Uppsala, Sweden

R. E. Johnson
Department of Nuclear Engineering and Engineering Physics, University of Virginia, Charlottesville, Virginia 22901

B. G. Svensson
Solid State Electronics, The Royal Institute of Technology, P.O. Box 1298, S-164 28 Kista-Stockholm, Sweden

(Received 24 April 1991; accepted for publication 6 June 1991)

The production of stable vacancy-related point defects in silicon irradiated with 1.3 MeV protons has been studied as a function of ion flux (protons $s^{-1} cm^{-2}$), while keeping the total fluence constant. Since the total fluence was very low (5×10^9 protons cm^{-2}), no interference between neighboring ion tracks was expected. The defect concentrations have been measured by deep-level transient spectroscopy, and a decrease in the resulting defect density is found for increasing flux. This effect was unexpected and shows that there is an overlap between ion tracks, in spite of the low fluence. The behavior is attributed to the rapidly diffusing silicon interstitials, which overlap the vacancy distributions produced in adjacent ion tracks. When the ion flux is low, the distribution of vacancies from one ion becomes diluted and recombination with interstitials from ions impacting at a later time is rare. As the flux is increased the vacancy distribution from one ion will still be confined to a small volume when it is overlapped by interstitials from a later ion, leading to an increased recombination of vacancies and interstitials. Thus, within this low-fluence regime, the total concentration of stable vacancy-related defects decreases for a high flux. This result is supported by computer simulations of the defect generation kinetics.

I. INTRODUCTION

Various types of irradiations, such as γ rays, electrons, and ions, have been used over the years to create damage and modify the properties of silicon. Generally the evolution of damage, or point defects, depends on the ion fluence and not the ion flux, although in the region of high fluences ($> 10^{14}$–10^{15} cm^{-2}), an increased flux is known to enhance defect production. However, the effect described in the present work has, to the best of our knowledge, never been reported. We have found a low-fluence regime where the rate of defect production is inversely proportional to the ion flux.

In this investigation a constant fluence of MeV protons (5×10^9 cm^{-2}) is used to generate defects in silicon at room temperature. These defects can be considered to be "secondary" since they are formed during the wake of diffusing "primary" defects, i.e., vacancies and interstitials, created directly in the collision events associated with an ion impact. Previous studies have revealed a fluence dependence for the creation of secondary defects,[1] but in the present study, the total proton fluence is kept constant while the flux (protons $s^{-1} cm^{-2}$) is varied. The defects investigated in this study are all electron traps in the upper part of the band gap in *n*-type silicon. They are the vacancy-oxygen center, the divacancy, known to have two charge states in the upper half of the band gap, and a trap related to the implanted protons.[2–6] The results of the experiment show that the production of these defects is inversely proportional to the flux, i.e., the production yield of secondary defects decreases with an increasing flux. The number of secondary defects is reduced by almost a factor of 10 within the investigated flux interval (10^7–2×10^{10} $s^{-1} cm^{-2}$).

Analysis of the samples was performed with deep-level transient spectroscopy (DLTS),[7] which has greatly increased the knowledge of the electrical activities of point defects in semiconductors. The method allows a characterization of deep levels by their band-gap position and capture cross sections, and together with other techniques such as infrared spectroscopy and electron paramagnetic resonance, the identities of point defects can be established. Furthermore, DLTS makes it possible to detect low concentrations of defects (10^{-6} below the background doping level is well within the detection limit) and to measure the concentration as a function of depth from the sample surface. The ability to measure depth profiles of defect concentrations is particularly convenient for the study of defects induced by ion irradiation since most of the defects are located at the end of the ion tracks deep beneath the surface.

In order to obtain a better understanding of the kinetics of defect migration and interactions, a one-dimensional computer model was developed. The computer model simulates the generation and diffusion of primary defects and the most important reactions between these mobile defects

 0021-8979/91/063025-06$03.00

TABLE I. The irradiations were carried out at room temperature with a scanned 1.3-MeV proton beam and the following irradiation parameters.

Group	Flux (protons/cm^2 s)	Irradiation time (s)	Fluence (protons/cm^2)
A	1.25×10^7	400	5.0×10^9(± 5%)
B	3.31×10^8	15.1	5.0×10^9(± 5%)
C	1.59×10^9	3.14	5.0×10^9(± 5%)
D	5.31×10^9	0.94	5.0×10^9(± 10%)
E	2.37×10^{10}	0.21	5.0×10^9(± 25%)

leading to stable, immobile secondary defect complexes. The results of the simulations are in qualitative agreement with experimental data, e.g., it is possible to explain the decrease in secondary defects as the flux is increased.

This investigation of radiation-induced defects is of great utility to the silicon device industry, as MeV proton irradiations can be used to modify charge carrier lifetimes in silicon.[8–10] This study indicates the importance of considering both the fluence and the flux when optimizing the lifetime of carriers in bulk silicon components. A low flux will yield a higher concentration of defects per incoming ion which, in the case of lifetime modification, is desirable. The findings may also be of importance for other cases of low-fluence irradiations where secondary defects are undesirable, since it demonstrates the possibility of minimizing the production of secondary defects by using a high flux.

II. EXPERIMENT

A. Preparation of samples

Diodes for the DLTS measurements were fabricated from high-purity float-zone silicon with an n-dopant concentration $N_D = 3 \times 10^{13}$ P/cm^3 employing neutron transmutation doping. This low doping level enables the depletion region of the diodes to extend deeper than the proton range, but it also sets an upper limit for the irradiation fluence, since the total density of traps, N_T, should not exceed 10% of N_D in order for the DLTS formalism to be valid. After implantation of 40-keV boron ions and a subsequent anneal, a p^+n junction was formed at a depth of approximately 1 μm. More details of the fabrication procedures can be found in Ref. 1.

The 1.3-MeV proton irradiation of the diodes was performed using the tandem accelerator at the The Svedberg Laboratory in Uppsala, where a beam line is equipped with an XY-scanning facility for homogeneous area coverage.[11] The energy corresponds to a mean projected range of 20 μm according to TRIM (Transport of Ions in Matter[12]) calculations. The irradiations were performed at nominal room temperature, and the fluxes and irradiation times employed are listed in Table I. The beam is switched off by an automatic beam stop that operates at high speed. The error in irradiation time introduced by the beam stop is estimated to be ~0.05 s, which accounts for the poor accuracy in the irradiation labeled E in Table I. However, for longer irradiation times this error is negligible and the accuracy is limited by fluctuations in the beam current, $\leqslant$5% at most.

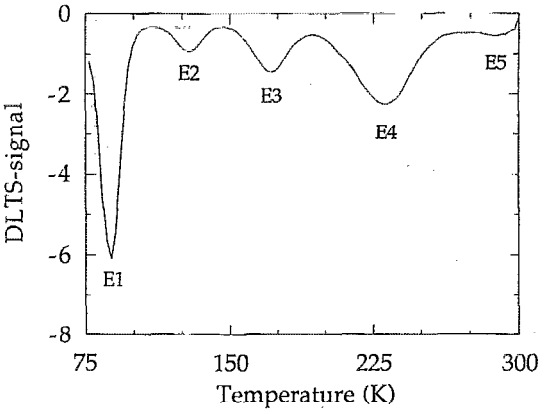

FIG. 1. DLTS majority-carrier spectrum of proton-irradiated n-type silicon from irradiation C. The repetition frequency used for the spectra was 100 Hz, the pulse duration was 100 μs, and the pulse amplitude 13 V (− 15 to − 2 V). The origin of the different peaks are as follows: E1, vacancy-oxygen complex; E2, divacancy (double negative charge state); E3, hydrogen-related defect; E4, divacancy (single negative charge state); and E5, hydrogen-related defect.

B. DLTS measurements

The spectrometer is a Semi-Trap DLS82E (Ref. 13) including a 1-MHz capacitance bridge, a LN_2-cooled cryostat with a chromel-alumel thermocouple, and a lock-in amplifier. The setup also includes a double-pulse generator used for direct depth profiles measurements by differential DLTS. A GP-IB interface transfers the measured data to a desk-top computer from which plotting and analysis are performed. The spectra were recorded with a repetition frequency of 100 Hz, 15 V reverse bias, and a filling pulse amplitude of 13 V and 100 μs duration. The depth concentration profiles were obtained with a second filling pulse having 1 V less amplitude than the first pulse, but of equal duration, applied during the second half of the lock-in period.

III. RESULTS

A typical DLTS spectrum of majority-carrier (electron) traps is shown in Fig. 1 (from irradiation C, Table I). Five traps can be seen and these have been identified elsewhere[3–8] as follows: E1, vacancy-oxygen complex (VO); E2, divacancy of doubly negative charge state (VV^{2-}); E3, hydrogen related; E4, divacancy of singly negative charge state (VV^{1-}); and E5, hydrogen related. The filling pulses are not long enough to completely saturate E5, which has a small cross section for electron capture, so E5 gives only a small contribution to the spectra. The total number of defects is directly related to the DLTS peak amplitudes, since the whole proton range is within the depleted region.

The distribution of E4 as a function of depth is shown in Fig. 2 for irradiations B and D. From the figure it can be seen that the difference between irradiation B and D is most pronounced in the region of maximum defect density. Closer to the surface it is difficult to distinguish between the two irradiations. In Fig. 3 the total (integrated) con-

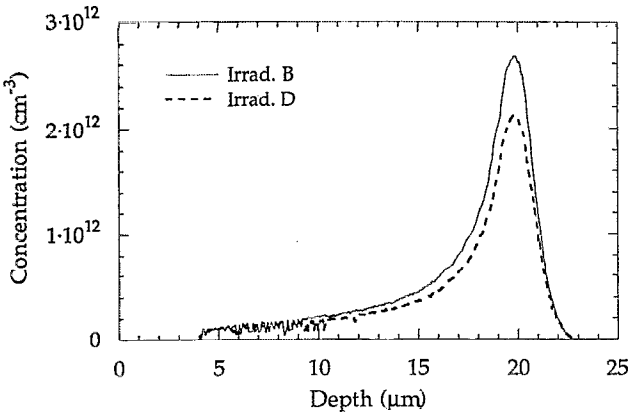

FIG. 2. Depth concentration profiles of E4 for two fluxes. The profiles have been recorded with the differential DLTS technique and a repetition frequency of 100 Hz.

centrations of defects E1–E4, deduced from DLTS peak amplitudes, are compared as a function of flux. The decrease of defects with increasing flux is seen throughout the investigated range, although a threshold seems to be reached at around $5 \times 10^9\ s^{-1}\ cm^{-2}$.

IV. SIMULATIONS

In order to further explore the inverse relation between flux and the production of secondary defects, a simple model of the defect generation was constructed, in which the following reactions are accounted for:

$$V + I \rightarrow 0 \text{ (annihilation)}, \quad (1)$$

$$V + V \rightarrow VV, \quad (2)$$

$$VV + I \rightarrow V, \quad (3)$$

$$V + O \rightarrow VO, \quad (4)$$

$$VO + I \rightarrow O \quad (5)$$

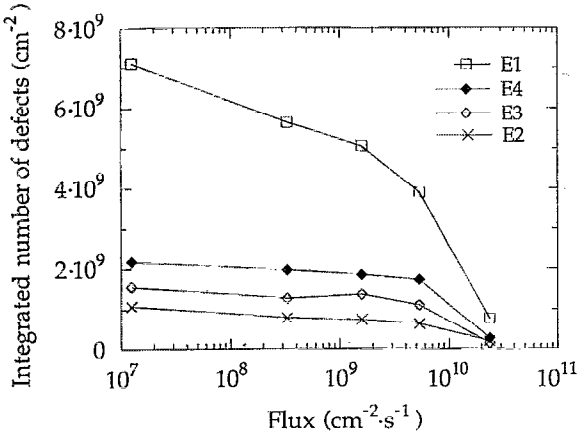

FIG. 3. Integrated number of secondary defects as a function of proton flux.

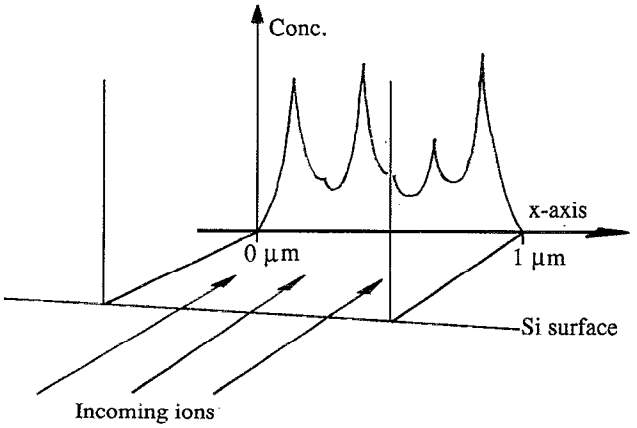

FIG. 4. Geometry of the simulations. Incoming ions generate primary defects on the x axis at a depth corresponding to the mean projected range. The primary defects are then allowed to move along this axis and form a stable distribution of secondary defects.

where V is a vacancy, I is the silicon interstitial, O is the interstitial oxygen atom, VV is the divacancy center, and VO is the vacancy-oxygen center. This set of equations is not complete, and several reactions which affect the absolute concentration of generated defects are omitted, e.g., formation of the carbon-oxygen-divacancy complex (the K center), carbon-carbon pairs, carbon-oxygen pairs, and direct generation of divacancy centers. However, the calculations are used here only as qualitative support to the experiments and more sophisticated models are required to obtain better quantitative agreement.

Other models of the defect kinetics of irradiated silicon concern MeV electron irradiation.[14,15] In that case the primary defects are distributed uniformly in the lattice and diffusion due to a concentration gradient can be neglected. For ions this is not the case and, in fact, the vacancies and interstitials can, in the first approximation, be considered to originate from a point source from which they spread radially. In the present calculations, the damage cascade from an incoming proton is simulated with a step function 50 Å wide and containing 1×10^{18} vacancies and interstitials per cm^3 (estimated from TRIM calculations[12]). The vacancies and interstitials are allowed to diffuse in one dimension in a direction perpendicular to the direction of incidence (see Fig. 4). The reaction rate between two defects A and B is determined by an effective capture radius, R, and the diffusion coefficients, $D_{A,B}$, according to $4\pi(D_A + D_B)R$. The oxygen concentration is set to $5 \times 10^{16}\ cm^{-3}$ and the following numbers are used for the constants[14]: $D_I = 3.2 \times 10^{-4}\ cm^2/s$, $D_V = 4.2 \times 10^{-9}\ cm^2/s$, and $R = 5$ Å. The rate equations are listed in Table II, where brackets denote concentrations and $\delta_{I,V}(x,t)$ are the source terms for primary defects.

The set of coupled equations is solved simultaneously from time $t = 0$, when the first cascade is initiated, until the vacancies from the last incident ion have disappeared. The time step used in the calculations is 2×10^{-10} s as long as interstitials are present, but when only vacancies are left, a time step of 2×10^{-5} s is sufficient. The step in

TABLE II. Set of simultaneous differential equations for reactions 1–5. Brackets denote concentrations and V, I, and O stand for vacancy, silicon interstitial, and interstitial oxygen, respectively. Diffusion constants for vacancies are given by D_V and for interstitials by D_I, while R is an effective capture radius. $\delta_{V,I}(x,t)$ are the source terms for vacancies and interstitials. The constants used in the simulations are $D_I = 3.2 \times 10^{-4}$ cm^2/s, $D_V = 4.2 \times 10^{-9}$ cm^2/s, and $R = 5$ Å.

$$\frac{d[V]}{dt} = \delta_V(x,t) + D_V\frac{d^2[V]}{dx^2} + 4\pi R D_I[I][VV] - 8\pi R D_V[V]^2 - 4\pi R(D_V + D_I)[I][V] - 4\pi R D_V[V][O]$$

$$\frac{d[I]}{dt} = \delta_I(x,t) + D_I\frac{d^2[I]}{dx^2} - 4\pi R D_I[I][VV] - 4\pi R(D_V + D_I)[I][V] - 4\pi R D_I[I][VO]$$

$$\frac{d[VV]}{dt} = 8\pi R D_V[V]^2 - 4\pi R D_I[I][VV]$$

$$\frac{d[VO]}{dt} = 4\pi R D_V[V][O] - 4\pi R D_I[I][VO]$$

$$\frac{d[O]}{dt} = [O] - 4\pi R D_V[V][O] + 4\pi R D_I[I][VO]$$

space is 50 Å, the simulated distance is 1.0 μm, and the vacancy and interstitial concentrations are set to zero for $x = 0.0$ and 1.0 μm. The sources for vacancies and interstitials, $\delta_{I,V}(x,t)$, are distributed randomly along the x axis with a density corresponding to the total fluence and separated in time with a constant delay, Δt, which corresponds to the average arrival rate of ions associated with the flux. The use of a scanned ion beam makes it difficult to estimate the fluxes for the one-dimensional simulations. The beam is scanned with a horizontal frequency of 517 and 64 Hz in the vertical direction; the beam spot has a diameter of around 3 mm and the scanned area is 7×7 cm^{-2}. From these values the time between incoming ions corresponding to the irradiations A–E in Table I are approximated to vary between 1 and 10^{-4} s μm^{-2}, respectively. The mean distance between ions for a fluence of 5×10^9 cm^{-2} is 0.15 μm.

Results from a simulation with six incoming ions are shown in Figs. 5(a) and 5(b) for E1 and E4, respectively. The order in which the ions have impacted is also indicated in the figure. E4 is the divacancy which is formed by pairing of two vacancies. In Figs. 5(a) and 5(b) it can be seen that the distribution of E4 is more localized to the regions where the density of vacancies was high, in contrast to E1. This indicates that the concentration of divacancies is proportional to the square of the concentration of vacancies, while E1, formed by pairing of vacancies and oxygen, is linear in vacancy concentration.

The integrated numbers of secondary defects E1 and E4 are plotted in Fig. 6 as a function of the frequency of ion impacts, given by $(\Delta t)^{-1}$. This number is found by integrating the distributions of simulated secondary defects, such as the one shown in Fig. 5, for seven different $(\Delta t)^{-1}$.

The simulations do not show as strong a dependence of secondary defect production on the flux as do the experiments, i.e., the decrease in the computed concentrations is

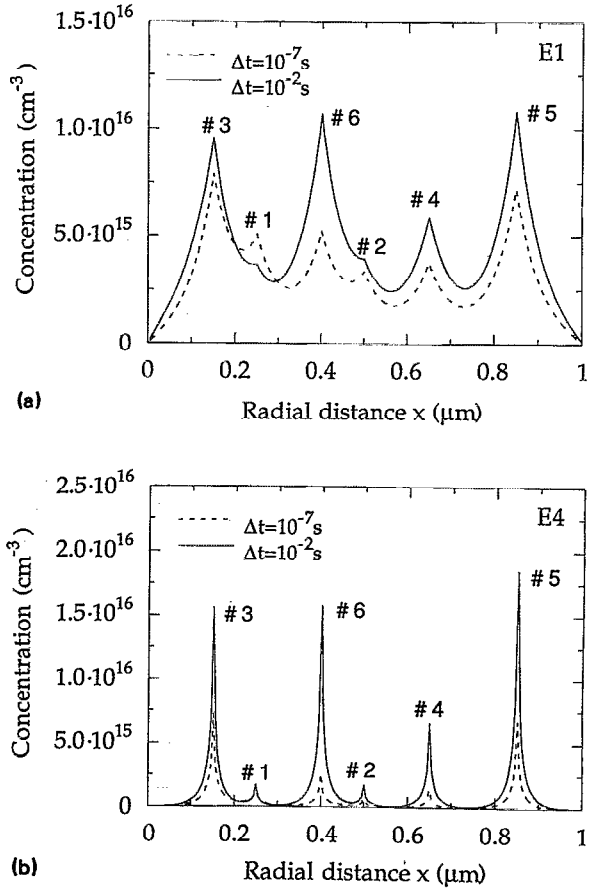

FIG. 5. Simulated distribution of (a) E1 and (b) E4 for two different fluxes. For the dashed curves, $\Delta t = 1 \times 10^{-7}$ s (the time between incoming ions), and for the full lines, $\Delta t = 1 \times 10^{-2}$ s. The order of the incoming ions is also shown.

at most 50%, while the measured values decrease to around 10% of the maximum concentration for the highest flux. In Fig. 6 the concentration is also seen to saturate to a constant value for the high fluxes, instead of dropping further. This saturation is associated with the finite range

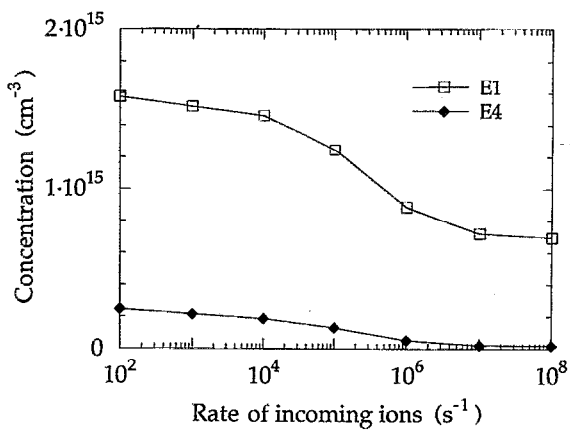

FIG. 6. Simulated total number of defects created in a layer perpendicular to the direction of incidence at the depth of the mean projected range as a function of the mean time between incoming ions.

used in the simulations as well as with the boundary condition employed: $[I(x,t)] = 0$ for $x = 0$ and 1 μm. Simulations carried out with the same six incoming ions, but with $0 < x < 4.0$ μm, reproduced the 90% decrease for E1. The reduction for divacancies (E4) is then even more pronounced.

The simulated total concentrations are also in disagreement with the measured concentrations at the end of range, seen in Fig. 2. For the lowest flux the simulated results are several hundred times larger than for the divacancy concentration (E4) in Fig. 2. (The E1 concentration profile is not included, since the concentration at the end of the proton range for this defect is larger than the limit, set by the DLTS formalism, of 10% of the background doping.) However, if the vacancies were allowed to diffuse in three dimensions, the number of defects at the end of the range would undoubtedly decrease and simulated values would agree better with experimental data. The concentration of impurity oxygen also affects the number of secondary defects and, as mentioned previously, adding reactions involving carbon as well as taking extended defects into account would further improve the model.

V. DISCUSSION

The low total fluence prevents overlap of the collision cascades themselves. However, the experiment as well as the simulations show that there is a strong dependence of secondary defect yield on the flux (protons s^{-1} cm^{-2}) which implies that species from adjacent ion tracks must interact. Considering the high diffusion constant for interstitials, we believe that the interstitials from one ion track recombine with the vacancies from adjacent tracks, causing a decrease in the total number of vacancy-related defects. (The interstitials and vacancies in one cascade will of course also recombine, but this occurs independently of the flux.) It is the decrease of vacancies at neighboring cascades due to recombination with interstitials from the last incoming ion that causes the *decrease* in vacancy concentration as the flux is *increased*. If the flux is very low, the vacancies have time to diffuse and disappear "by themselves" at other lattice imperfections and no flux dependence of the production of secondary defects is seen.

This effect is quite in contrast to experiments using higher generation rates for primary defects (by using heavier ions and total fluences in excess of 10^{14} cm^{-2}), where the opposite flux dependence have been reported; the accumulation of damage *increases* with an *increasing* flux.[16] The explanation for this correlation is that the vacancy distributions from consecutive ions are so close, both in time and space, that they overlap and cause an enhancement in the production of secondary defects.

One can also speculate about the direct generation of divacancies (E4). From the experiment (Fig. 3) it can be seen that the decrease is slightly more pronounced for E1 than E4, but from the simulations (Fig. 6) E4 is more affected by the higher flux. This indicates that there is a direct generation of E4 by the incoming ions, which has not been accounted for in the model. Of course the formation of divacancies by pairing of two vacancies must be the dominant process, otherwise there would be no flux dependence.

The importance of different reaction channels was also investigated by excluding them from the differential equations. If the recombination of vacancies and interstitials [reaction (1)] is excluded, the production yield of secondary defects increases with increasing flux. This result further supports our explanation that it is the recombination between vacancies and nearby interstitials (close both in time and space) that causes the measured decrease of secondary defects as the flux is increased. If the channels (3) and (5) ($VV + I \rightarrow V$ and $VO + I \rightarrow O$, respectively) are excluded, the simulations will still give a decrease in yield for an increased flux. The decrease of divacancies is in this case, however, less pronounced than the decrease of vacancy-oxygen complexes, since in (3) an already formed divacancy dissolves and liberates a vacancy that is free to form either a new divacancy or an oxygen-vacancy complex. If this reaction is prevented, the production of divacancies is less sensitive to an increased flux.

VI. CONCLUSIONS

The production yield (per incoming proton) of secondary point defects, such as the vacancy-oxygen and the divacancy, is shown to decrease with increasing proton flux. The lower yield can be explained by an overlap of the vacancy distribution created by an incident ion and the interstitial distribution due to an ion stopped nearby (near both in time and space). An increased flux causes this overlap to increase, enhancing the annihilation of vacancies and interstitials and decreasing the production of secondary defects. This effect is only seen if the generation rate of primary defects is kept low, and we employed incident fluxes between 10^7 and 10^{10} protons cm^{-2} s^{-1}. If higher fluxes are used, the vacancy distributions from ions penetrating nearby in space and time begin to overlap and the flux dependence of the production yield will be the opposite, i.e., the yield of secondary defects will increase with increasing dose rate.

ACKNOWLEDGMENTS

We are grateful to Dr. Curt T. Reimann for his valuable comments on the manuscript. Partial financial support was provided by the Swedish Board for Technical Development.

[1] A. Hallén, Z. Paska, M. Rosling, B. U. R. Sundqvist, B. G. Svensson, and J. Tirén, J. Appl. Phys. **67**, 1266 (1990).
[2] L. C. Kimerling, P. Blood, and W. M. Gibson, in *Defects and Radiation Effects in Semiconductors*, edited J. H. Albany, Inst. Phys. Conf. Ser. No. 46 (Institute of Physics, Bristol, 1978), p. 273.
[3] K. Irmscher, H. Klose, and K. Maass, J. Phys. C **17**, 6317 (1984).
[4] A. O. Evwaraye and E. Sun, J. Appl. Phys. **47**, 3776 (1979).
[5] B. G. Svensson, A. Hallén, and B. U. R. Sundqvist, J. Mater. Sci. Eng. B **4**, 285 (1989).
[6] M. Hüppi, Mater. Sci. Forum **38-41**, 177 (1989).
[7] D. Lang, J. Appl. Phys. **45**, 3023 (1974).
[8] D. C. Sawko, and J. Bartko, IEEE Trans. Nucl. Sci. **30**, 1756 (1983).
[9] A. Mogro-Campero, R. P. Love, M. F. Chang, and R. F. Dyer, *IEEE* Trans. Electron Devices **33**, 1667 (1986).

[10] A. Hallén and M. Bakowski, Solid-State Electron. **32**, 1033 (1989).
[11] A. Hallén, P. A. Ingemarsson, P. Håkansson, G. Possnert, and B. U. R. Sundqvist, Nucl. Instrum. Methods B **36**, 345 (1989).
[12] J. P. Biersack and L. G. Haggmark, Nucl. Instrum. Methods **174**, 257 (1980).
[13] G. Ferenczi, P. Krispin, and M. Somogyi, J. Appl. Phys. **54**, 3902 (1983).
[14] G. S. Oehrlein, I. Krafcsik, J. L. Lindström, A. E. Jaworowski, and J. W. Corbett, J. Appl. Phys. **54**, 179 (1983).
[15] S. Mottet and A. Roizes, in *Defects and Radiation Effects in Semiconductors*, edited by J. H. Albany, Inst. Phys. Conf. Ser. No. 46 (Institute of Physics, Bristol, 1978), p. 281.
[16] A. Claverie, A. Roumili, N. Gessinn, and J. Beauvillain, J. Mater. Sci. Eng. B **4**, 205 (1989).